Gland segmentation in gastric histology images: detection of intestinal metaplasia

Panagiotis Barmpoutis[1,2], William Waddingham[2], Christopher Ross[2], Kayhanian Hamzeh[2], Daniel C. Alexander[1], Marnix Jansen[2]

[1]Department of Computer Science, University College London, UK
[2]Department of Pathology, University College London, UK

***Abstract*— Gastric cancer is one of the most frequent causes of cancer-related deaths worldwide. Gastric intestinal metaplasia (IM) of the mucosa of the stomach has been found to increase the risk of gastric cancer and is considered as one of the precancerous lesions. Therefore, early detection of IM may have a valuable role in histopathological risk assessment regarding the possibility of progression to cancer. Accurate segmentation and analysis of gastric glands from the histological images plays an important role in the diagnostic confirmation of IM. Thus, in this paper, we propose a framework for segmentation of gastric glands and detection of IM. More specifically, we propose the GAGL-Net for the segmentation of glands. Then, based on two features of the extracted glands we classify the tissues into normal and IM cases. The results showed that the proposed gland segmentation approach achieves an F1 score equal to 0.914. Furthermore, the proposed methodology shows great potential for the IM detection achieving an accuracy score equal to 96.6%. To evaluate the efficiency of the proposed methodology we used a publicly available dataset and we created the GAGL dataset consisting of 59 Whole Slide Images (WSI) including both IM and normal cases.**

Keywords*— *Gastric cancer, medical image segmentation, intestinal metaplasia detection.

I. Introduction

Gastric cancer is a major public health issue. As reported by the WHO in 2020 [1], it remains one of the most common cancers (sixth most frequent type) and it is the fourth leading cause of cancer-related deaths mainly due to its often-late stage of diagnosis [2]. The risk factors of gastric cancer include Helicobacter pylori infection, salt intake, smoking, alcohol, family history of gastric cancer, gastric atrophy and intestinal metaplasia (IM) [2], [3], [4]. In particular, several studies suggest that IM of the mucosa of the stomach is a major precursor lesion of gastric cancer [5], [6]. For this reason, the early and effective diagnosis of IM is a crucial step to prevent gastric cancer. In IM, the metaplastic glands replace the native gastric glands and Paneth cells, goblet cells and absorptive cells appear. Widely used diagnostic methods for IM include endoscopic and histological diagnosis. Endoscopic diagnosis of extensive IM is reliable, but there are difficulties in making the diagnosis of mild IM cases. Biopsy confirmation for staging suspected cases of IM remains the gold standard approach. To this end, based on the Sydney protocol [7], the features of IM are identified and are visually confirmed by histopathologists.

However, the visual assessment of IM glands by histopathologists is a labour and time-consuming task [8], with a degree of inter-observer variability even with standardised classification systems [9]. Thus, automated precise segmentation and classification of glands from histological images could play an important role in glandular morphology analysis, which is a crucial criterion for IM effective detection and management. This could be a labour and cost saving technology, with potential to improve diagnostic reliability. Numerous methods have been proposed in literature for gland segmentation. However, to date, no generally applicable digital pathology approach has been proposed and applied for the segmentation of gastric glands and identification of either mild or moderate cases of intestinal metaplasia. Towards this end, in this paper, we propose a methodology for gastric glands segmentation and IM detection based on Hematoxylin and Eosin (H&E) -stained whole slide image (WSI). More specifically, this paper makes the following contributions:

- We propose the GAGL-Net model consisting of two branches for the extraction of global and local multi-scale features and segmentation of gastric glands.
- We introduce a digital pathology framework exploiting the automated gland segmentation for the early detection of IM cases.

The rest of this paper is organized as follows: First, related works are discussed. Then, details of the proposed methodology are presented, followed by experimental results using the GAGL dataset. Finally, some conclusions are drawn and future extensions are discussed.

II. Related Works

The digital medical image segmentation and classification field receives growing attention and has become more and more popular [10]. Thus, various techniques and methods, based on either hand-crafted or deep learning features, have been developed for histopathological image segmentation and classification tasks. Hand-crafted developed methodologies use a low-level or mid-level set of features to represent an image or regions of this. More specifically, glands segmentation, based on identification and growing of candidate lumen regions [8], on different scales analysis [11] and on construction and quantification of object-glands, [12] has been utilized. In other approaches epithelial nuclei identification has been performed and used for gland segmentation [13].

On the other hand, more sophisticated classification techniques methods such as deep-learning techniques [14] and higher-order dynamical systems [15] have been developed aiming to address histopathological image segmentation and classification problems by extracting high-level features and knowledge directly from the data. More specifically, Chen et al. [16] proposed a deep contour-aware network aiming to focus more on the boundaries' segmentation among glands. This is based on a fully convolutional network consisting of two different branches and three weighted auxiliary classifiers aiming to enhance the discrimination capability and to strengthen the training optimization process. Xu, et al. [17] proposed a deep multichannel side supervision model combining foreground segmentation, edge detection and object detection channels, for instance segmentation in gland histology images. Furthermore, Graham et al., [18] used minimal information loss units incorporating the original down-sampled image into the residual unit aiming to retain

maximal information that is essential for segmentation. On the other hand, Yan, et al. [19] used a unified model and focused on the training of it through a shape-preserving loss function for both pixel-wise gland segmentation and boundary detection. More recently, a multi-scale fully convolutional network extracting different receptive field features was proposed [20]. In the latter, the authors used three-class classification and two branches in order to both achieve boundary segmentation and retain the global information.

III. Materials and Methods

The framework of the proposed methodology for the gastric glands segmentation and classification of WSI into normal and IM cases is shown in Fig. 1. Initially, a WSI image is divided into blocks and fed into the GAGL-Net for the training of the gland segmentation model. Then, based on the estimated glands, two features of the segmented glands are extracted and an SVM classifier is used for the detection of intestinal metaplasia cases.

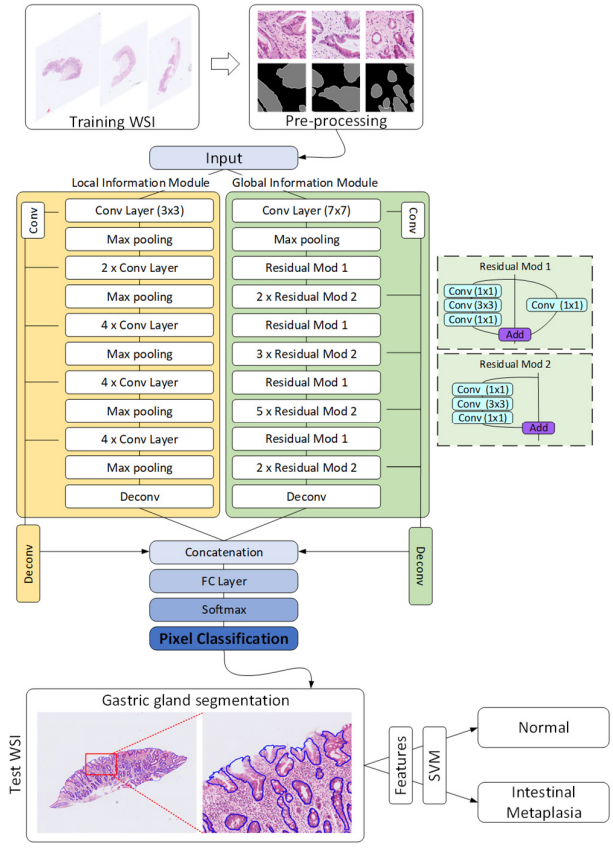

Fig. 1. The proposed methodology. GAGL-Net model receives as input gastric WSI and it performs segmentation of gastric glands. Detection of IM glands is performed through the extraction of two features and the deployment of an SVM classifier.

A. Dataset description

To evaluate the efficiency of the proposed methodology we created a dataset consisting of 59 WSI (Fig. 2). More specifically, the dataset includes 14 normal and 45 IM images. Gastric tissues were collected at University College London Hospital NHS trust, with ethical approval (research ethics committee (REC) reference: 15/YH/0311, & 19/LO/0089) with informed consent taken for prospective tissue collection. The tissues underwent routine haematoxylin & eosin (H&E) staining. For the training of the GAGL-Net model we used 10 annotated WSI while for the validation we used 12 annotated WSI (testing dataset). The rest of the WSI, which are unannotated with regards to glands, were used for the analysis of gastric biopsies. It is worth mentioning that, as our aim is to develop a methodology for the early detection and diagnosis of IM to prevent gastric cancer, in this dataset we included mild and moderate IM cases.

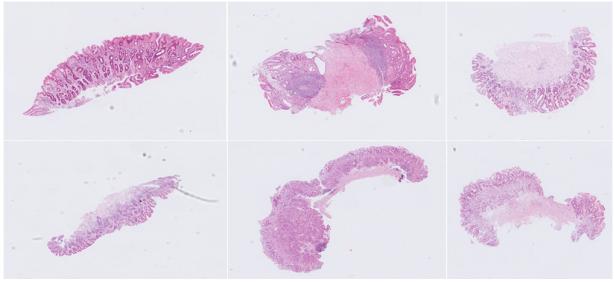

Fig. 2. Sample gastric tissue images of the GAGL dataset.

B. Gland segmentation

Gland instance segmentation is a complex task that requires the extraction of meaningful global and local features. Thus, in the proposed method, similarly to previous classification approaches [21], [22], we combine two branches extracting different receptive field features and multi-level contextual features using digitized images of H&E stained gastric tissue slides. More specifically, the proposed GAGL-Net model comprises a local module inspired by the DCAN [16] and a global module inspired by the ResNet-50 [23] enabling the exploitation of both local and global information. The GAGL-Net model includes a downsampling path and an upsampling path, and integrates a series of modifications aiming to achieve good performance and computation efficiency. In the local module the input image patches with size of $480\times480\times3$ pass through a 3×3 conventional convolution layer while in the global module they pass through a 7×7 convolution layer. For the further utilisation of both contextual information and finer details in both modules we extract different receptive field features as shown in Fig. 1. Thus, more low-level information is retained and multi-size gland segmentation is achieved. It is worth mentioning that in some malignant cases the previous developed models achieve lower segmentation scores on degenerated and elongated glands. This would be a drawback in the case of analysis glands and gastric pits of IM. Thus, the proposed model aims to increase the overall detection accuracy of glands in WSI by extracting features from the global module, while the local module increases the segmentation performance. Finally, the corresponding feature maps are up-sampled with deconvolutional layers and they are concatenated for pixel classification. The details of GAGL-Net are shown in Fig. 1. It should be noted that all the convolutional layers are followed by the batch normalization and ReLU activated function.

Furthermore, for the enrichment of the training data of the GAGL network for the task of gastric gland segmentation we utilized the transfer learning technique. For transfer learning, a pre-trained neural network is fine-tuned to a target dataset. More specifically, we initialized the layers in the down-sampling path with the pre-trained weights from the VGG-19 and ResNet-50 models parameters and then the whole GAGL-Net model was fine-tuned with training data prepared for this work. In addition, an augmentation method was utilized to

further increase the variability of the training dataset and to avoid overfitting of the network. In particular, we included translation, rotation and flipping transformations.

For the training of our model, three-class labelled images (created on pre-processing step) were used in order to produce both the segmentation masks of gland objects and contours. The three classes represent the following categories: background, gland lumen, and gland edge. Additionally, a modified loss function was defined using a class weighting to balance the classes:

$$Loss = L2 - \sum_{p=1}^{N} w_p r_p \log(t_p) \quad (1)$$

where w_p , r_p and t_p denote the weighting factors, the reference values and the predicted values at pixel p respectively, and N is the total number of pixels. L2 denotes the regularization term. Stochastic Gradient Descent (SGD) was used to optimize the loss function. The initial learn rate was defined as 0.005, the weight decay as 0.01 and the momentum as 0.9. The network was trained on a single NVIDIA GeForce RTX 3090 GPU with batch size 10 for 50 epochs. For the testing, overlap-tile strategy was used for gland segmentation of WSI. Then, post-processing steps including filling holes and removing small areas are performed.

C. Detection of intestinal metaplasia

Having estimated the masks of gastric glands, we extract two features for the discrimination of WSI of gastric biopsies into normal and IM glands. More specifically, in order to model and to translate the pathologist's knowledge into a universally reproducible set of mathematical values for the IM recognition we estimated the average number of glands and the average area of glands per WSI of gastric biopsies. For the detection of IM cases, the calculated features for each WSI are fed into an SVM classifier. More specifically, after the normalization of the data we used an SVM classifier implemented with the Gaussian kernel.

IV. Results and Discussion

In this section, we present a detailed evaluation analysis of the proposed gastric gland segmentation as well as the classification of normal and IM cases. The goal of this experimental evaluation is threefold. Initially, we compared the efficiency of gland segmentation, using a widely used colon dataset and state of the art approaches. Secondly, we used the GAGL dataset in order to validate the proposed model for the identification of gastric glands on normal and IM cases. Finally, we applied our methodology to the WSI gastric dataset in order to classify and analyze the gastric WSI and determine whether significant associations could be found between the glandular features of normal and IM cases.

For the evaluation of the proposed method, three evaluation metrics were employed, namely F1 score, object dice and object Hausdorrf. The F1 score is defined as:

$$F1 = \frac{2 \cdot Precision \cdot Recall}{(Precision + Recall)} \quad (2)$$

where Precision is $N_{TP}/(N_{TP} + N_{FP})$, Recall is $N_{TP}/(N_{TP} + N_{FN})$, N_{TP} is the number of true positive, N_{FP} is the number of false positives and N_{FN} is the number of false negatives. The F1 score corresponds to detection accuracy while the object Dice is defined as follows:

$$D_{Object}(G,S) = \frac{1}{2}\left[\sum_{i=1}^{n_s}(|S_i|/\sum_{p=1}^{n_s}|S_p|)D(G_{iMax},S_i) + \sum_{j=1}^{n_G}(|G_j|/\sum_{q=1}^{n_G}|G_q|)D(G_j,S_{jMax})\right] \quad (3)$$

where D is the Dice index of G and S and it is equal to $D(G,S) = 2(|G \cap S)|)/(|G| \cup |S|)$. G is the ground truth image and S is the segmented image. The object Dice corresponds to segmentation performance. The object Hausdorrf is defined as:

$$H_{Object}(G,S) = \frac{1}{2}\left[\sum_{i=1}^{n_s}(|S_i|/\sum_{p=1}^{n_s}|S_p|)H(G_{iMax},S_i) + \sum_{j=1}^{n_G}(|G_j|/\sum_{q=1}^{n_G}|G_q|)H(G_j,S_{jMax})\right] \quad (4)$$

where H is the Hausdorrf distance of G and S and it is equal to:

$$H(G,S) = Max\begin{pmatrix} sup_{x\in G} inf_{y\in S}\|x-y\| \\ sup_{y\in S} inf_{x\in G}\|x-y\| \end{pmatrix} \quad (5)$$

Sup represents the supremum and inf the infimum. The object Hausdorrf corresponds to shape similarity. Higher score values of F1 and object Dice as well as lower scores of object Hausdorrf indicate better performance.

A. A comparison of state-of-the-art methods: GLAS dataset

In this section, using a well-known dataset containing H&E-stained colorectal cancer tissue images we aim to present a comparison of the proposed methodology against a number of different gland segmentation approaches. More specifically, we used the Gland Segmentation (GlaS) challenge dataset used as part of MICCAI 2015 [8]. This dataset was acquired by a team of pathologists at the University Hospitals Coventry and Warwickshire in United Kingdom. It contains 165 histological images that were extracted from 16 H&E-stained WSI. The dataset is split into the training set including 85 images (37 benign and 48 malignant), and the testing sets consisting of part A and part B which include 60 (33 benign and 27 malignant) and 20 images (4 benign and 16 malignant) respectively.

Table I. Performance comparison	**F1 Score**		**Object Dice**		**Object Hausdorff**	
	Part A	**Part B**	**Part A**	**Part B**	**Part A**	**Part B**
CVML [8]	0.652	0.541	0.644	0.654	155.43	176.24
LIB [8]	0.777	0.306	0.781	0.617	112.71	190.45
FCN-8 [24]	0.783	0.692	0.795	0.767	105.04	147.28
SegNet [25]	0.858	0.753	0.864	0.807	62.62	118.51
DeepLab v3 [26]	0.862	0.764	0.859	0.804	65.72	124.97
Freidburg2 [8]	0.87	0.695	0.876	0.786	57.09	148.47
Manivannan et al. [27]	0.892	0.801	0.887	0.853	51.175	**86.987**
Xu et al. [17]	0.893	0.843	0.908	0.833	44.13	116.82
ExB3 [8]	0.896	0.719	0.886	0.765	57.36	159.87
CUMedVision2 [16]	0.912	0.716	0.897	0.781	45.42	160.35
MILD-Net [18]	0.914	0.844	0.913	0.836	41.54	105.89
TCC-MSFCN [20]	0.914	0.850	0.913	**0.858**	**39.84**	93.24
Yan et al. [19]	**0.924**	0.844	0.902	0.840	49.881	106.075
GAGL-Net	0.918	**0.855**	**0.915**	0.854	41.48	98.96

More specifically, in Table 1, we present the evaluation results of the GAGL-Net model in comparison to thirteen state-of-the-art methods. This analysis reveals that GAGL-Net is amongst the top three performing methods. More precisely, the proposed model towards gland segmentation achieves F1

score rates of 91.8% and 85.5% for part A and part B test sets respectively. The achieved F1 score for part A is the second best rate while for part B the proposed model achieves the top performance. Similarly, the achieved object Dice rates are 0.915 and 0.858 for part A and part B respectively. These rates correspond to the top performance and to the second best score against the compared methods respectively. Moreover, the proposed model achieves object Hausdorff scores of 41.48 and 98.96 corresponding to the third best performances for both part A and part B test sets.

It is worth mentioning that the proposed GAGL-Net model introduces a global and a local branch extracting different receptive field features from each one. Thus, as depicted in Table I, our model offers an improved F1 Score for malignant cases as well as a higher score in segmentation performance of benign cases. In contrast, although some models [19], [20], [27] achieve better shape similarity, they achieve lower detection and segmentation rates that would lead to incorrect results regarding the estimation of the number and area of glands that are used for the detection of IM cases. Fig. 3 illustrates qualitative results of the proposed model on the GlaS challenge dataset. It shows that the GAGL-Net model accurately identifies both benign and malignant glands. However, there is a limited number of cases where the lack of lumen (Fig. 3d) causes false negative results.

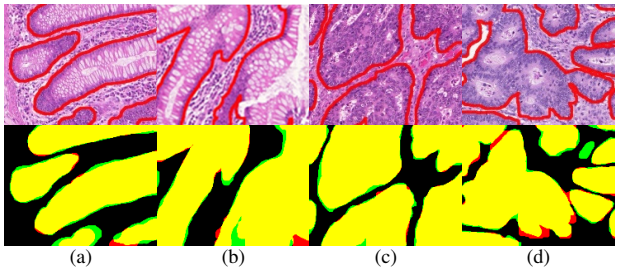

(a) (b) (c) (d)

Fig. 3. Gland segmentation results of GAGL-Net model on the GlaS challenge dataset in comparison with ground truth: Yellow color (True Positive), red color (False Positive), green color (False Negative).

B. *Gastric glands segmentation results: GAGL dataset*

Subsequently, in order to confirm that the performance of the proposed methodology remains robust in gastric tissues, we carried out a validation analysis using the GAGL dataset (Fig. 4). More specifically, we used 12 annotated WSI and the GAGL-Net model in order to perform segmentation of the gastric glands and the gastric pits.

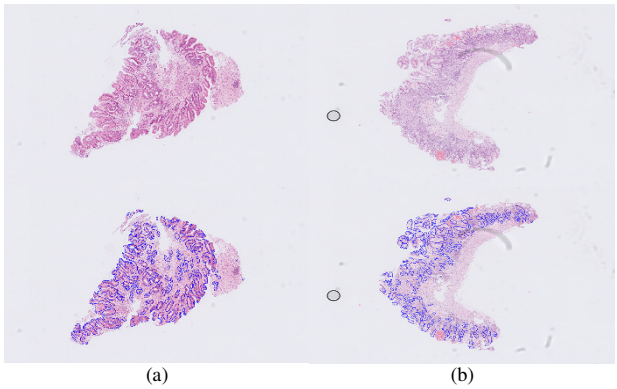

(a) (b)

Fig. 4. Gland segmentation results of GAGL-Net model on two sample WSI of the GAGL dataset.

The results show that the proposed gland segmentation approach achieves F1 score equal to 0.914 and object Dice score equal to 0.908. Moreover, the proposed model achieves object Hausdorff score equal to 44.12. Similarly to the GlaS dataset, results in the GAGL dataset (Fig. 4) show the great potential of the proposed model which is capable of identifying glands with high shape and size diversity. However, there is a limited number of small glands and gastric pits that are not accurately detected due to either the small size of the glands or image artefacts (Fig. 5).

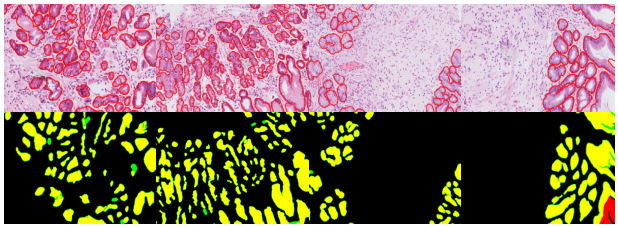

(a) (b) (c) (d)

Fig. 5. Detailed gland segmentation results of GAGL-Net model on the GAGL dataset.

C. *Gastric biopsies analysis*

In this work, features of the segmented glands were used for the analysis of gastric biopsies. Initially, we estimated the number of glands for normal and IM cases (Fig. 6). More specifically, the average number of glands in normal cases is 551.5 (median is equal to 390.1) and the average number of glands in IM cases is 302.1 (median is equal to 271.1).

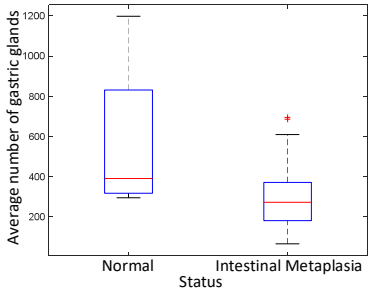

Fig. 6. Average number of gastric glands per WSI of gastric biopsies.

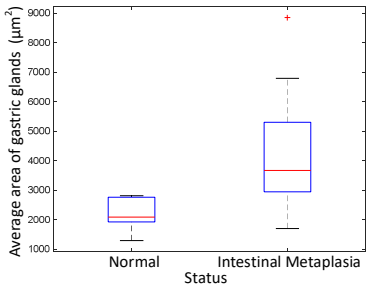

Fig. 7. Average area of gastric glands per WSI of gastric biopsies.

In additional analyses, we estimated the average area of glands for normal and IM cases (Fig. 7). For the normal cases we identified that the average area of glands in normal cases is 2137.6μm^2 (median is equal to 2079.3) and the average number of glands in IM cases is 4113.2μm^2 (median is equal to 3667.6). The aforementioned results validate the Sydney protocol and the fact that IM cases are usually associated with extensive atrophy carrying an increased risk of malignancy.

Moreover, we used the extracted features and an SVM classifier aiming to classify the gastric tissues into normal and IM cases. Our model achieves 96.6% accuracy score showing great potential for automated identification of mild and moderate IM cases. Finally, we internally validated the efficiency for IM identification by performing an ablation analysis. The individual use of the number and area of gastric glands achieve accuracy scores equal to 93.2% and 94.9% respectively.

V. Conclusion

Multiple risk factors and a multistep process have been associated with gastric carcinogenesis. Among these factors, gastric IM of the mucosa has been recognized as high-risk precancerous lesions for dysplasia and gastric cancer. In this paper we present a methodology for the automated segmentation of gastric glands and the classification of gastric tissues into normal and IM cases. The proposed GAGL-Net model for gastric glands segmentation achieves F1 score equal to 0.914, object Dice score equal to 0.908 and object Hausdorff score equal to 44.12. Furthermore, for the classification of the gastric tissues we extracted two features and we used an SVM classifier achieving 96.6% accuracy score. The results suggest that the proposed methodology obtains promising performance on the GAGL dataset and IM detection. The analysis of gastric glands reflects the expected results based on the Sydney scoring system. This model could have further applications in automated histopathological diagnosis and classification and may represent a potential avenue for significant cost and labour saving in the histopathology clinical diagnostic pathway. However, limitations of this study include the lack of individual gland classification that will assist us to accurately grade each WSI. Thus, a future step would be to use artificial intelligence for both glands segmentation and grading of gastric biopsies in order for the proposed framework to be adopted on a widespread basis in routine histopathological practice.

Acknowledgment

The EPSRC and CRUK support this work through joint funding in grant number NS/A000069/1.

References

[1] WHO, Cancer, [Online]. Available: https://www.who.int /news-room/fact-sheets/detail/cancer [Accessed: 25- Jan- 2022].

[2] Waddingham W, Nieuwenburg SA, Carlson S, Rodriguez-Justo M, Spaander M, Kuipers EJ, Jansen M, Graham DG, Banks M. Recent advances in the detection and management of early gastric cancer and its precursors. Frontline Gastroenterology. 2021 Jul 1;12(4):322-31.

[3] Peleteiro B, Lopes C, Figueiredo C, Lunet N. Salt intake and gastric cancer risk according to Helicobacter pylori infection, smoking, tumour site and histological type. British journal of cancer. 2011 Jan;104(1):198-207.

[4] Jencks DS, Adam JD, Borum ML, Koh JM, Stephen S, Doman DB. Overview of current concepts in gastric intestinal metaplasia and gastric cancer. Gastroenterology & hepatology. 2018 Feb;14(2):92.

[5] Busuttil RA, Boussioutas A. Intestinal metaplasia: a premalignant lesion involved in gastric carcinogenesis. Journal of gastroenterology and hepatology. 2009 Feb;24(2):193-201.

[6] Pellegrino C, Michele R, Chiara M, Alberto B, Florenzo M, Antonio N, Gioacchino L, Tiziana M, Gian LD, Francesco DM. From Sidney to OLGA: an overview of atrophic gastritis. Acta Bio Medica: Atenei Parmensis. 2018;89(Suppl 8):93.

[7] Dixon MF, Genta RM, Yardley JH, Correa P. Classification and grading of gastritis: the updated Sydney system. The American journal of surgical pathology. 1996 Oct 1;20(10):1161-81.

[8] Sirinukunwattana K, Pluim JP, Chen H, Qi X, Heng PA, Guo YB, Wang LY, Matuszewski BJ, Bruni E, Sanchez U, Böhm A. Gland segmentation in colon histology images: The glas challenge contest. Medical image analysis. 2017 Jan 1;35:489-502.

[9] Capelle LG, de Vries AC, Haringsma J, Ter Borg F, de Vries RA, Bruno MJ, van Dekken H, Meijer J, van Grieken NC, Kuipers EJ. The staging of gastritis with the OLGA system by using intestinal metaplasia as an accurate alternative for atrophic gastritis. Gastrointestinal endoscopy. 2010 Jun 1;71(7):1150-8.

[10] Barmpoutis P, Kayhanian H, Waddingham W, Alexander DC, Jansen M. Three-dimensional tumour microenvironment reconstruction and tumour-immune interactions' analysis. In: IEEE 2021 Digital Image Computing: Techniques and Applications (pp. 01-06).

[11] e Gonçalves WG, Dos Santos MH, Lobato FM, Ribeiro-dos-Santos Â, de Araújo GS. Deep learning in gastric tissue diseases: a systematic review. BMJ open gastroenterology. 2020 Mar 1;7(1):e000371.

[12] Sharma H, Zerbe N, Heim D, Wienert S, Behrens HM, Hellwich O, Hufnagl P. A multi-resolution approach for combining visual information using nuclei segmentation and classification in histopathological images. In: VISAPP (3) 2015 Mar 11 (pp. 37-46).

[13] Sirinukunwattana K, Snead DR, Rajpoot NM. A stochastic polygons model for glandular structures in colon histology images. IEEE Transactions on medical imaging. 2015 May 15;34(11):2366-78.

[14] Barmpoutis P, Di Capite M, Kayhanian H, Waddingham W, Alexander DC, Jansen M, Kwong FN. Tertiary lymphoid structures (TLS) identification and density assessment on H&E-stained digital slides of lung cancer. Plos one. 2021 Sep 23;16(9):e0256907.

[15] Dimitropoulos K, Barmpoutis P, Zioga C, Kamas A, Patsiaoura K, Grammalidis N. Grading of invasive breast carcinoma through Grassmannian VLAD encoding. PloS one. 2017 Sep 21;12(9):e0185110.

[16] Chen H, Qi X, Yu L, Dou Q, Qin J, Heng PA. DCAN: Deep contour-aware networks for object instance segmentation from histology images. Medical image analysis. 2017 Feb 1;36:135-46.

[17] Xu Y, Li Y, Wang Y, Liu M, Fan Y, Lai M, Eric I, Chang C. Gland instance segmentation using deep multichannel neural networks. IEEE Transactions on Biomedical Engineering. 2017 Mar 23;64(12):2901-12.

[18] Graham S, Chen H, Gamper J, Dou Q, Heng PA, Snead D, Tsang YW, Rajpoot N. MILD-Net: Minimal information loss dilated network for gland instance segmentation in colon histology images. Medical image analysis. 2019 Feb 1;52:199-211.

[19] Yan Z, Yang X, Cheng KT. A deep model with shape-preserving loss for gland instance segmentation. In International Conference on Medical Image Computing and Computer-Assisted Intervention 2018 Sep 16 (pp. 138-146). Springer, Cham.

[20] Ding H, Pan Z, Cen Q, Li Y, Chen S. Multi-scale fully convolutional network for gland segmentation using three-class classification. Neurocomputing. 2020 Mar 7;380:150-61.

[21] Cho KO, Lee SH, Jang HJ. Feasibility of fully automated classification of whole slide images based on deep learning. The Korean Journal of Physiology & Pharmacology. 2020 Jan 1;24(1):89-99.

[22] Bougourzi F, Dornaika F, Taleb-Ahmed A. Deep learning based face beauty prediction via dynamic robust losses and ensemble regression. Knowledge-Based Systems. 2022 Jan 31:108246.

[23] He K, Zhang X, Ren S, Sun J. Deep residual learning for image recognition. In: IEEE 2016 Computer Vision and Pattern Recognition (pp. 770-778).

[24] Long J, Shelhamer E, Darrell T. Fully convolutional networks for semantic segmentation. In: IEEE 2015 Computer Vision and Pattern Recognition (pp. 3431-3440).

[25] Badrinarayanan V, Kendall A, Cipolla R. Segnet: A deep convolutional encoder-decoder architecture for image segmentation. IEEE Transactions on pattern analysis and machine intelligence. 2017 Jan 2;39(12):2481-95.

[26] Chen LC, Papandreou G, Kokkinos I, Murphy K, Yuille AL. Deeplab: Semantic image segmentation with deep convolutional nets, atrous convolution, and fully connected crfs. IEEE transactions on pattern analysis and machine intelligence. 2017 Apr 27;40(4):834-48.

[27] Manivannan S, Li W, Zhang J, Trucco E, McKenna SJ. Structure prediction for gland segmentation with hand-crafted and deep convolutional features. IEEE transactions on medical imaging. 2017 Sep 8;37(1):210-21.